

Supporting Information

Janus gas: Reversible redox transition of Sarin enables its selective detection by an ethanol modified SnO₂ chemiresistor

By Zhengfei Dai,[†] Guotao Duan,^{†,*} Zhenxing Cheng,[‡] Lei Xu,[§] Tie Li,[§] Guangqiang Liu,[†] Hongwen Zhang,[†] Yue Li[†] and Weiping Cai^{†,*}

[†]Key Lab of Materials Physics, Anhui Key lab of Nanomaterials and Nanotechnology, Institute of Solid State Physics, Chinese Academy of Sciences, Hefei, 230031, Anhui, China.

[‡]The No. 3 Department, Institute of Chemical Defence, Beijing, 102205, China.

[§]State Key Laboratory of Transducer Technology, and the Science and Technology on Micro-system Laboratory, Shanghai Institute of Microsystem and Information Technology, Chinese Academy of Sciences, Shanghai, 200050, China.

E-mail: duangt@issp.ac.cn; wpcai@issp.ac.cn.

S1. Fabrication of the supporting system of the device.

The IDEs-microheater chip was fabricated based on classic MEMS processes.^{S1} (i) A double-side-polished 350µm-thickness N-type <100> oriented silicon wafer with a layer of SiO₂ (200 nm in thickness) thermally grown at 1100 °C; (ii) Then a SiO₂ (400 nm in thickness)/Si₃N₄ (600 nm in thickness) membrane was successively deposited on each side of the silicon substrate by low pressure chemical vapor deposition (LPCVD) at 800 °C; (iii) A nanolayer Al₂O₃ with a thickness of 10 nm was deposited by atomic layer deposition (ALD) and patterned by ion-beam etching; (iv) The Pt/Ti electrodes (10 µm wide and 10 µm separated) and bonding pads were patterned by lift-off process with the adhesive Al₂O₃ layer buried beneath Pt; (v) Then the SiO₂/Si₃N₄ membrane was selectively etched by Ion-beam to form front etching windows and the membrane was released in a solution of TMAH (25 wt.%) at 80 °C. So far, the microheater was prepared. (vi) Then, a SiO₂ (600 nm in thickness) layer, a insulating layer, was deposited on it by plasma enhanced chemical vapor deposition (PECVD); (vii) The Pt/Au interdigital electrodes (10 µm wide and 10 µm spacing, 200 nm in thickness) and leading wires were patterned by lift-off process. (viii) Positive photolithography was used to define the corrosion windows for releasing the heating membrane area and the support cantilever; (ix) Under the protection of the photoresist, the exposed silicon oxide and silicon nitride composite membrane were etched completely using

reactive ion etching (RIE); (x) Silicon substrate was etched through the release windows using KOH etching solution, forming the inverted trapezoidal insulation cavity. By now, the IDEs-microheater MEMS-based chip was fabricated.

Figure S1 Zhengfei Dai *et al.*

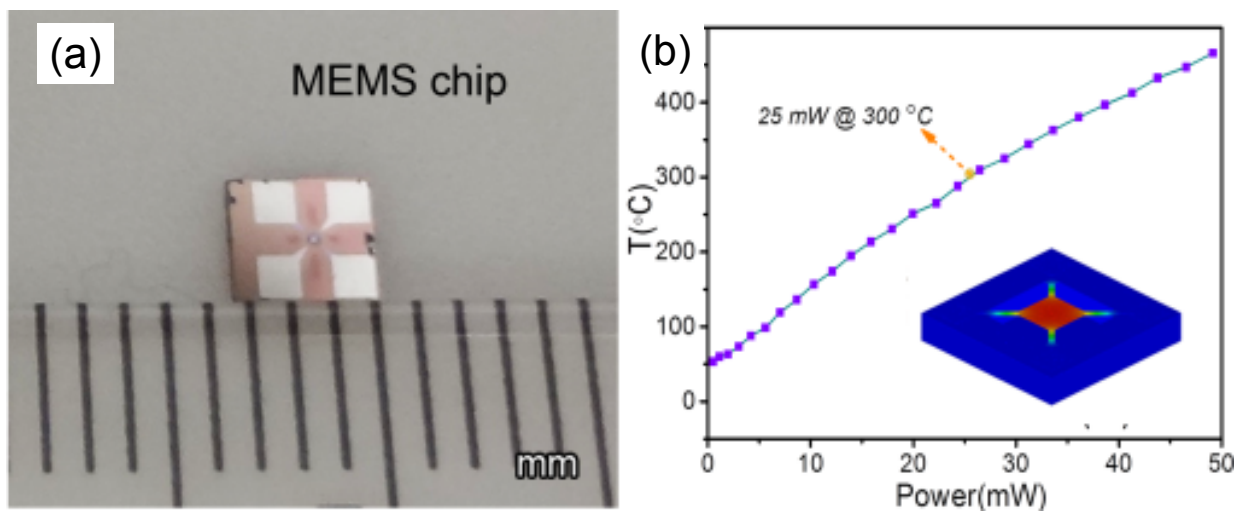


Figure S1. A typical photo (a) and (b) the heating power consumption of the MEMS chip.

S2. Fabrication process of MEMS based SnO₂ sensor

Glass slides (7.5×2.5 cm²), with 2 mm in thickness, were cleaned according to the procedures reported previously.^{S2} Suspension of monodispersed PS with 200 nm in diameters (2.5 wt % in water, surfactant-free) was obtained from Alfa Aesar Corporation. The PS colloidal monolayer template was prepared on the well cleaned glass slide by air/water interfacial assembly (Figure S2).^{S3} A 0.02 M SnCl₄ aqueous solution was used as the precursor solution. Based on the route of solution-dipping and transferring the template shown in Figure S3, the PS monolayer floating on the solution surface was picked up with a desired substrate (MEMS-based chip) from the solution, and flat-placed for 10 min and then dried at 120 °C for 0.5 h in an oven. Subsequently, we picked up another floated PS monolayer using such dried PS-covered IDEs chip and then heating at 400 °C for 2 h. By now, a double-layer porous SnO₂ sensing film was in situ produced on the MEMS-based IDEs chip to construct a gas sensor. Owing to the better stability, we chose the double-layer porous SnO₂ sensing film rather than monolayer.

Figure S2 Zhengfei Dai *et al.*

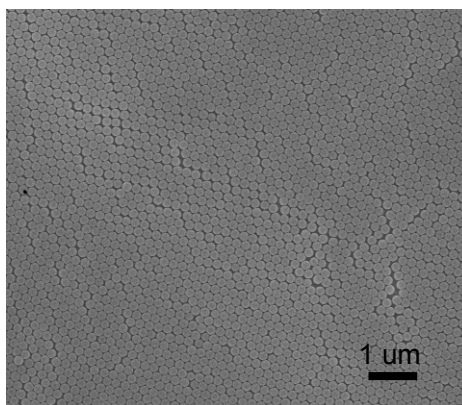


Figure S2. SEM image of a PS sphere (200 nm in diameter) monolayer. The morphologies and microstructures of the samples were examined on a field-emission scanning electron microscope (FESEM, Sirion 200)

Figure S3 Zhengfei Dai *et al.*

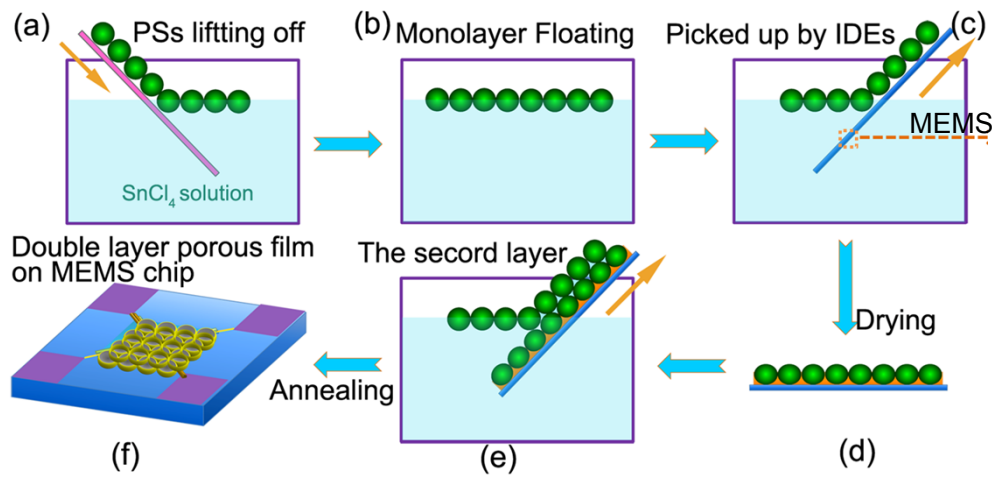


Figure S3. Fabrication process of MEMS based SnO₂ sensor. (a) A flat glass slide covered with a PS sphere (200 nm in diameter) monolayer is slowly dipped into a SnCl₄ solution. (b) The colloidal monolayer floats on the surface of the solution. (c) The floating monolayer is picked up using a MEMS-based chip. (d) The MEMS-based chip covered with the monolayer is placed for drying. (e) Subsequently, another floated PS monolayer was picked up by the dried sample and then heating at 400 °C for 2 h.

S3. Structure of the MEMS based SnO₂ sensor

Figure S4 clearly displays the as-synthesized double-layer ordered porous SnO₂ film. It indicates that the SnO₂ film is honeycomb-shaped, and all the spherical pores are in a hexagonal arrangement.

Figure S4 Zhengfei Dai *et al.*

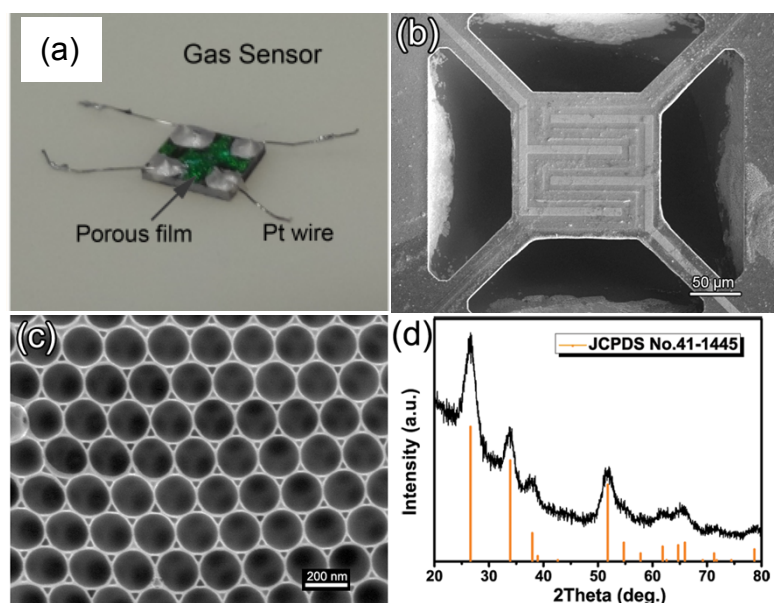


Figure S4. (a) A photograph of as-fabricated sensor. (b) The morphology of the as-fabricated MEMS-based SnO₂ film gas sensor structure. (c) Enlarged view corresponding to the area marked in (a), showing a honeycomb-shaped double-layer ordered nanoporous SnO₂ film. (d) XRD pattern of the as-obtained double-layer SnO₂ film, indicating a phase of tetragonal rutile (JCPDS No. 41-1445). Phase analysis of the films was carried out on a Philips X'Pert powder X-ray diffractometer using Cu K α (0.15419 nm) radiation.

S4. Schematic illustration of dynamical gas sensing system.

The device is enclosed in a gas flow chamber, with its electrodes connected to a capture card (Agilent mod. U3606A). The analyte–gas mixture is produced in a gas generator in which Figure S5: a stream of air gas is split into three parts by the flow adjustment 1, 2 and 3, and the flow rate agree: $\text{flow1} + \text{flow2} = \text{flow3}$. Flow 1 is led through a flow chamber containing an sarin permeation tube and then mixed with flow 2 with different relative content for different sarin concentrations. During a measurement, a continuous gas stream of constant flow rate, which can be switched between air (flow 3 for sensing recovery) and sarin–air mixture, is directed over the device.

The sensing response was obtained by measuring the change of the electrical voltage of the sensing devices. Using Labview software, the heating voltages in the sensing devices were controlled and data were acquired. All the measurements, if no specification, were conducted at the relative humidity 50% and the room temperature 25°C ambient.

Figure S5 Zhengfei Dai *et al.*

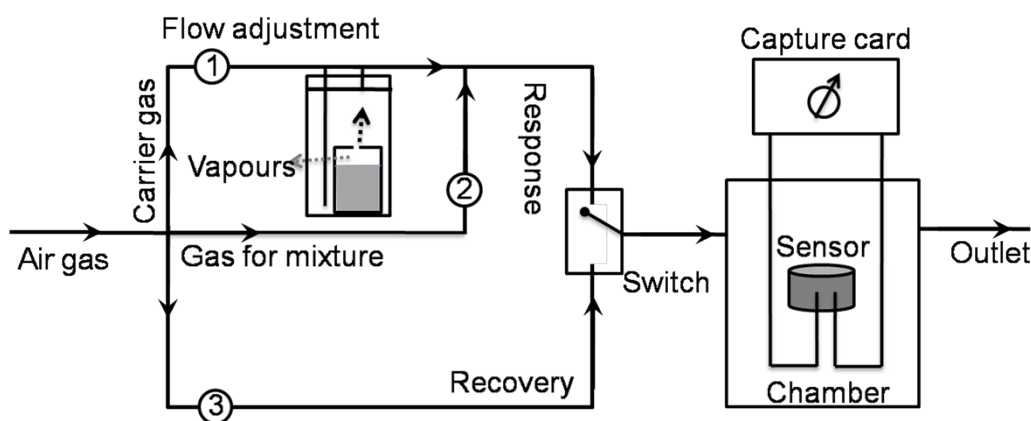


Figure S5. Schematic illustration of dynamical gas sensing system.

Figure S6 Zhengfei Dai *et al.*

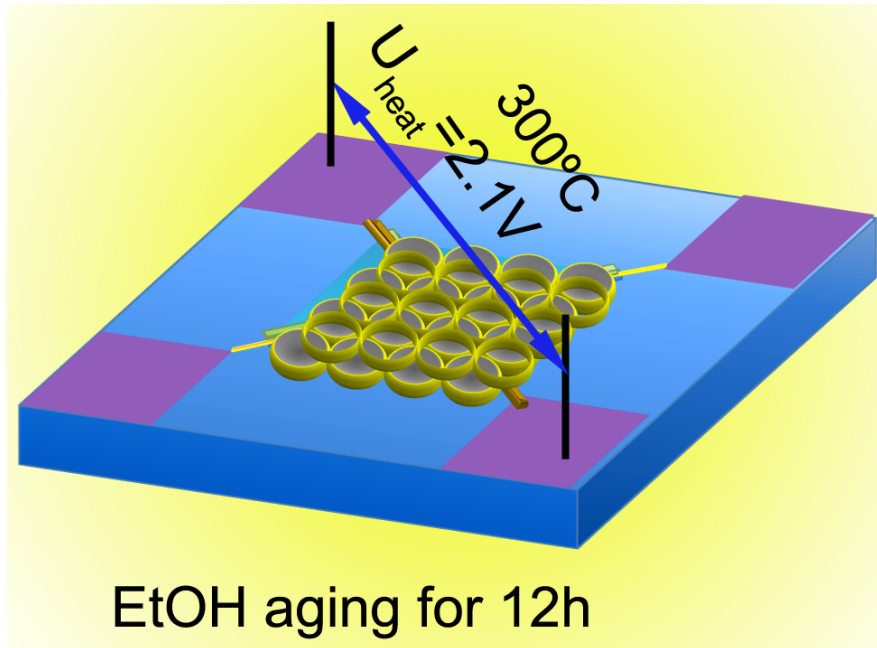


Figure S6. The schematic illustration of 12 hours aging of the SnO_2 sensor under 100 ppm EtOH at 300°C corresponding to 2.1 V heating voltage imposed to the microheater.

Figure S7 Zhengfei Dai *et al.*

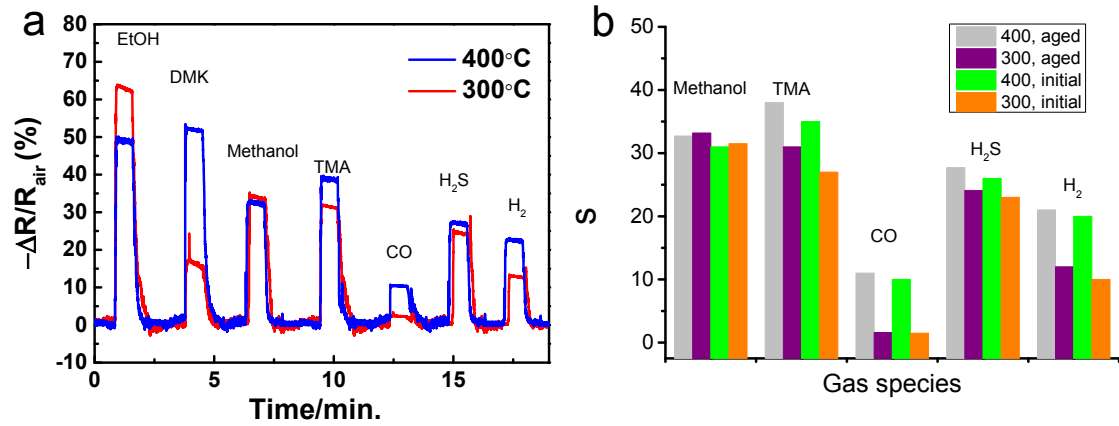


Figure S7. (a) Gas-sensing performances of the EtOH-aged MEMS-based SnO₂ sensor at 300~400°C, 50%RH to 1 ppm acetone (DMK) and EtOH, methanol, Trimethylamine (TMA), CO, H₂S and H₂, respectively. (b) The bar graph summarizing the sensitivities of the initial and aged sensors to 1 ppm different gas at 300~400°C, 50%RH, respectively.

Figure S8 Zhengfei Dai *et al.*

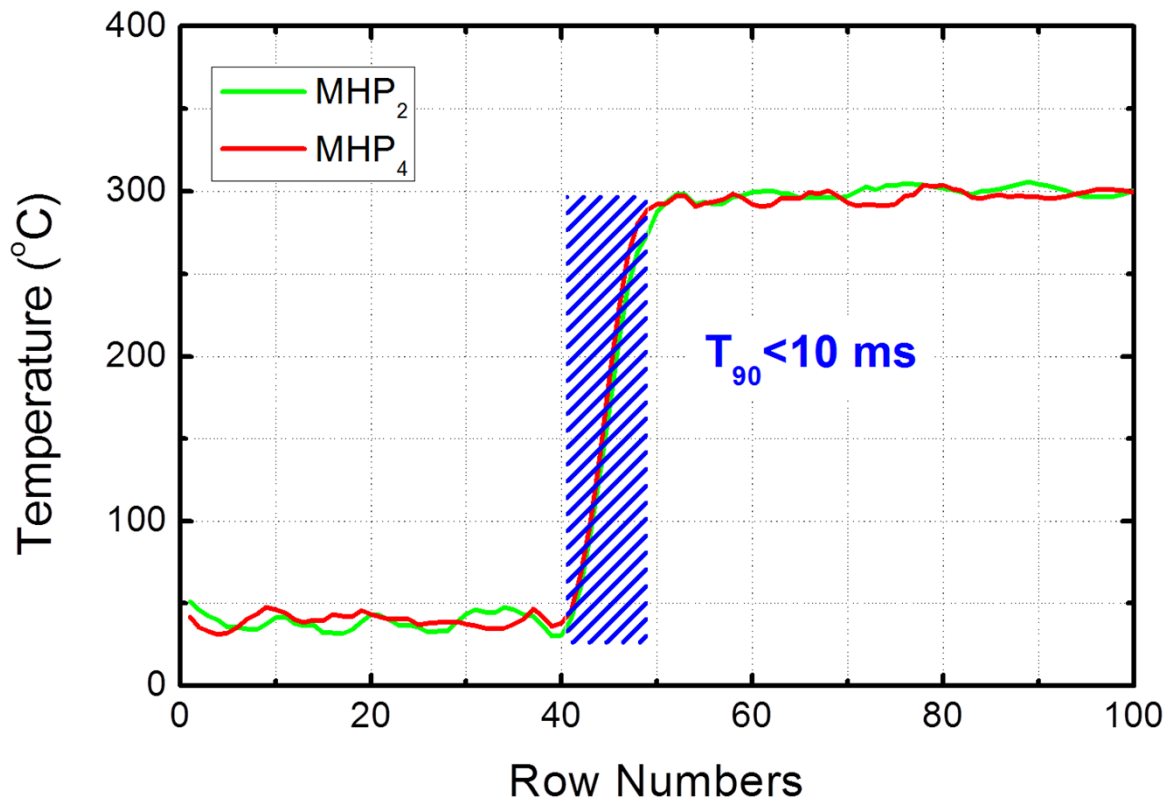


Figure S8. The response time of MEMS sensors to operating temperature. The heating response time was as short as 10 ms for the temperature increasing from room temperature to 300 °C due to the small thermal mass of the microheater. This feature is particularly useful when the sensor is operated in a pulse voltage mode, since these sensors are fast in warming up.

Figure S9 Zhengfei Dai

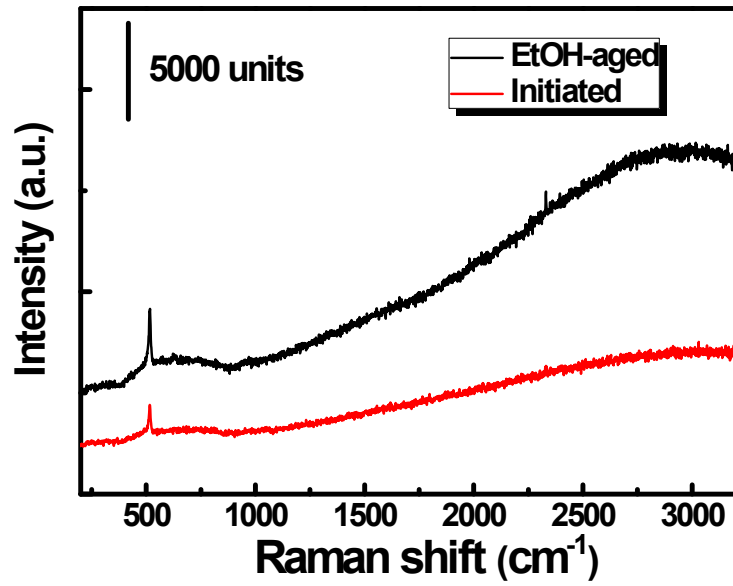


Figure S9. The Raman spectra of the initialed and EtOH-aged films, respectively. The Raman spectra were examined on a confocal microprobe Raman spectrometer (Renishaw inVia Reflex) with a laser beam of 633 nm wavelength, 5 mW power, and 5 seconds integral time.

Figure S10 Zhengfei Dai

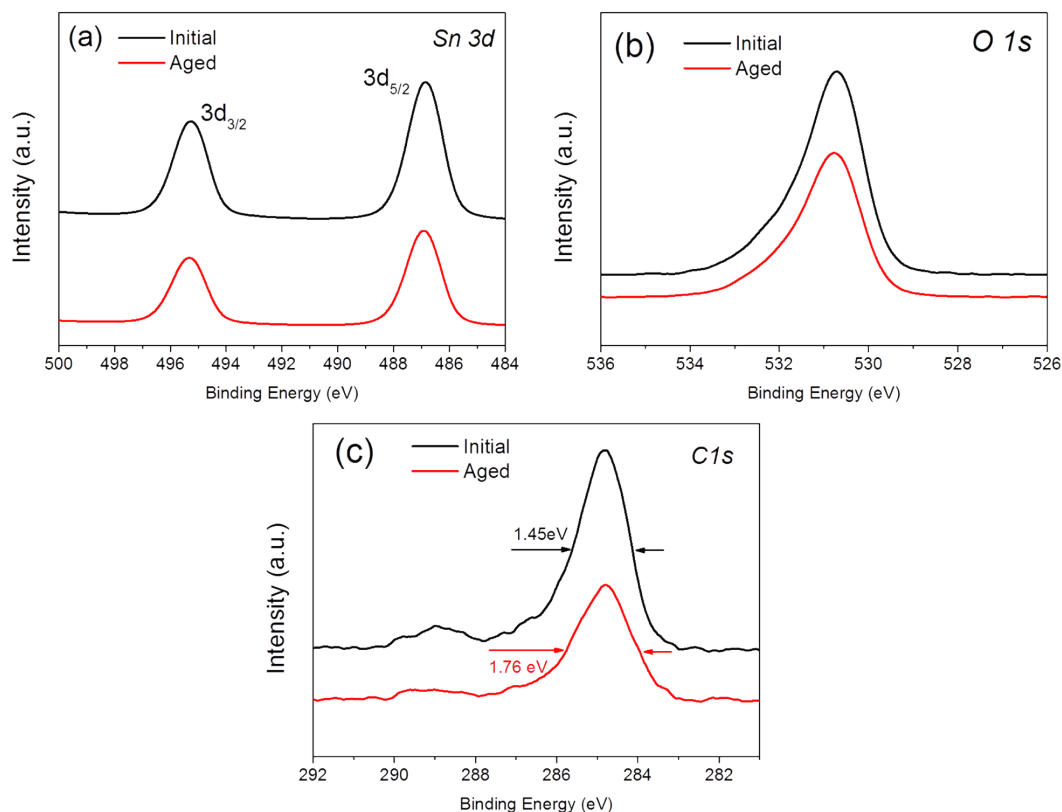


Figure S10. XPS spectra for the initial and EtOH-aged samples. (a) Sn 3d binding energy spectra. (b) O 1s core level spectra. (c) C 1s XPS spectra.

X-ray photoelectron spectrum (XPS) analysis was conducted using an Al K α X-ray source on a Thermo-VG ESCALAB MKII spectrometer. In (a) and (b), the peak position of Sn 3d and O 1s XPS spectra are almost same, indicating the same chemical components of the two SnO₂ samples. A C1s line at 284.75 eV is observed which has a full width at half maximum (FWHM) of 1.76 eV for the EtOH-aged sample (Figure S10c). The observed FWHM is larger than the FWHM of the C1s line for the initial sample (FWHM= 1.45 eV). The observed 0.31 eV binding energy shift would be in accordance with the chemical shift between sp^2 and sp^3 hybridized carbon species.^[S12] According to the literature,^[S13] the broadened C1s peak shape change may be due to C-H bond cleavage, which can be interpreted as a rehybridization from sp^2 to sp^3 resulting in the C-H bond formation.

Table S1. DMMP or sarin sensing responses of resistive semiconductors in the literature and in the present study.

| Sensing material | Morphology | Target gas | Gas conc. (ppb) | Response | T (°C) | Ref. |
|-------------------|-------------|------------|-----------------|----------|--------|-----------|
| Pt/ZnO | thick films | DMMP | 2000 | 95 | 450 | S4 |
| WO ₃ | nanodots | DMMP | 1000 | 5 | 450 | S5 |
| SnO ₂ | thick films | DMMP | 100 | 70 | 350 | S6 |
| SnO ₂ | nanobelts | DMMP | 53 | 1 | 500 | S7 |
| CNT/Polythiophene | Nanofibers | DMMP | 50 | 2 | 70 | S8 |
| SWCNT-CoPc | Nanotube | DMMP | 500 | 2 | RT | S9 |
| SnO ₂ | nanowires | DMMP | 200 | 3 | 500 | S10 |
| SnO ₂ | Thin film | DMMP | 200 | 4 | 400 | S10 |
| SWCNT | Nanotube | DMMP | 5000 | 2 | RT | S11 |
| SnO ₂ | Nanopores | Real Sarin | 6 | 36 | 400 | This work |
| SnO ₂ | Nanopores | Real Sarin | 6 | -5 | 300 | This work |

Abbreviation: SWCNT- single-walled carbon nanotubes (CNT)

Reference

- (S1) Z. Dai, L. Xu, G. Duan, T. Li, H. Zhang, Y. Li, Y. Wang, Y. Wang and W. Cai, *Sci. Rep.*, 2013, **3**, 1669.
- (S2) L. C.Jia, W. P. Cai, H. Q.Wang, F. Q.Sun, Y. Li, *ACS Nano* **2009**, *3*, 2697-2705.
- (S3) Z. Dai, Y. Li, G. Duan, L. Jia and W. Cai, *ACS Nano*, 2012, **6**, 6706-6716.
- (S4) L. A. Patil, A. R. Bari, M. D. Shinde, V. Deo and M. P. Kaushik, *Sensor. Actuators, B*, 2012, **161**, 372-380.
- (S5) A. Vergara, R. Calavia, R. Maria Vazquez, A. Mozalev, A. Abdelghani, R. Huerta, E. H. Hines and E. Llobet, *Anal. Chem.*, 2012, **84**, 7502-7510.
- (S6) S. C. Lee, S. Y. Kim, W. S. Lee, S. Y. Jung, B. W. Hwang, D. Ragupathy, D. D. Lee, S. Y. Lee and J. C. Kim, *Sensors (Basel)*, 2011, **11**, 6893-6904.
- (S7) C. Yu, Q. Hao, S. Saha, L. Shi, X. Y. Kong and Z. L. Wang, *Appl. Phys. Lett.*, 2005, **86**. 063101
- (S8) F. Wang, H. W. Gu and T. M. Swager, *J. Am. Chem. Soc.*, 2008, **130**, 5392-+.
- (S9) Y. Wang, N. Hu, Z. Zhou, D. Xu, Z. Wang, Z. Yang, H. Wei, E. S.-W. Kong and Y. Zhang, *J. Mater. Chem.*, 2011, *21*, 3779-3787.
- (S10) G. Sberveglieri, C. Baratto, E. Comini, G. Faglia, M. Ferroni, M. Pardo, A. Ponzoni and A. Vomiero, *Thin Solid Films*, 2009, **517**, 6156-6160.
- (S11) Y. Wang, Z. Zhou, Z. Yang, X. Chen, D. Xu and Y. Zhang, *Nanotechnology*, 2009, **20**, 345502.
- (S12) T.I.T. Okpalugo, P. Papakonstantinou, H. Murphy, J. McLaughlin, N.M.D. Brown, *Carbon*, 2005, **43**, 153–161.
- (S13) A. Nikitin, H. Ogasawara, D. Mann, R. Denecke, Z. Zhang, H. Dai, K. Cho and A. Nilsson, *Phys. Rev. Lett.*, 2005, **95**, 225507.